Soft Tunable Lenses Based on Zipping Electroactive Polymer Actuators

*Florian Hartmann, Lukas Penkner, Doris Danninger, Nikita Arnold,
and Martin Kaltenbrunner**

Compact and entirely soft optics with tunable and adaptive properties drive the development of life-like soft robotic systems. Yet, existing approaches are either slow, require rigid components, or use high operating voltages of several kilovolts. Here, soft focus-tunable lenses are introduced, which operate at practical voltages, cover a high range of adjustable focal lengths, and feature response times in the milliseconds range. The nature-inspired design comprises a liquid-filled elastomeric lens membrane, which is inflated by zipping electroactive polymers to tune the focal length. An analytic description of the tunable lens supports optimized designs and accurate prediction of the lens characteristics. Focal length changes between 22 and 550 mm (numerical aperture 0.14–0.005) within 260 ms, equal in performance to human eyes, are demonstrated for a lens with 3 mm aperture radius, while applying voltages below 500 V. The presented model, design rules, and fabrication methods address central challenges of soft electrostatic actuators and optical systems, and pave the way toward autonomous bio-inspired robots and machines.

Conventional imaging optics for smartphones and cameras require systems of multiple lenses and motors to change focal length and provide variable magnification. However, the excessive number of components increases device complexity, weight, and price. Nature-inspired optics that mimics the human eye enables soft tunable lens systems with reduced complexity, high compactness, and speed.[1,2] Realizing the essential functionality
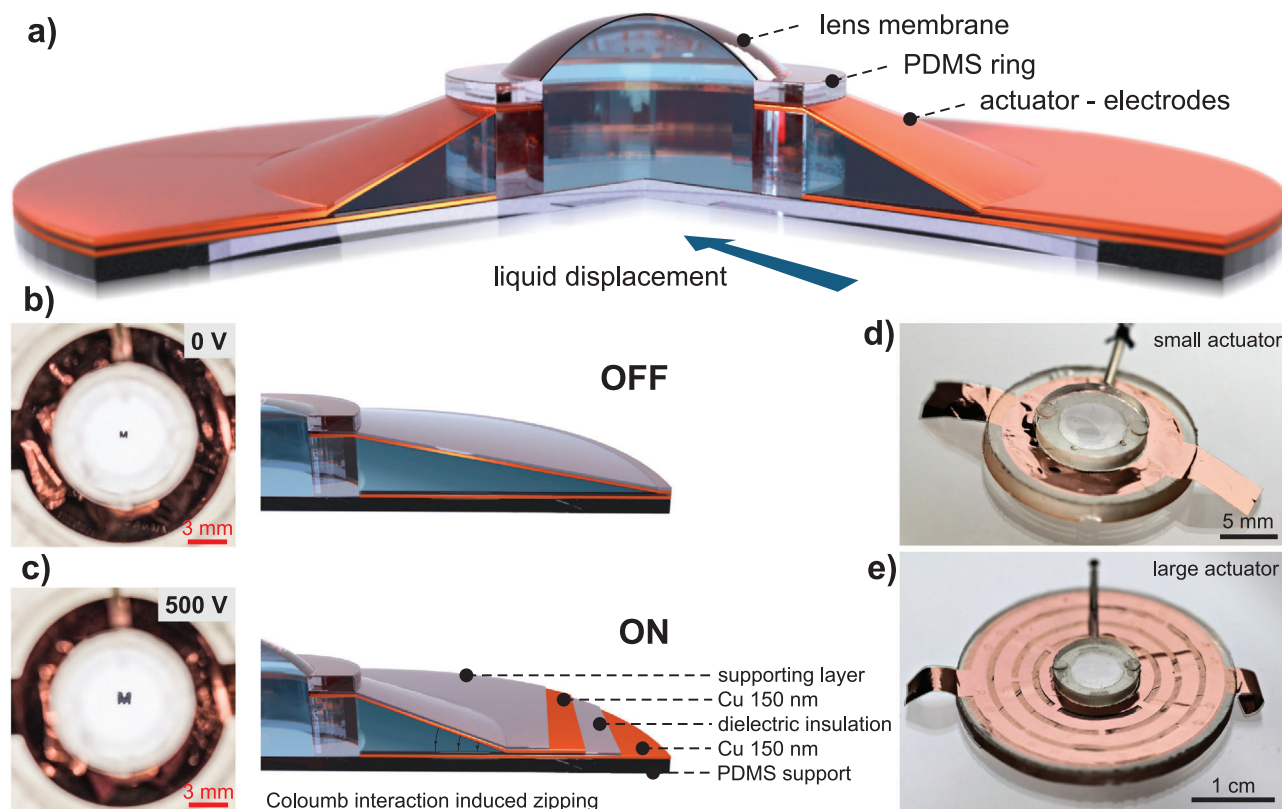
F. Hartmann, L. Penkner, D. Danninger, Dr. N. Arnold,
Prof. M. Kaltenbrunner
Division of Soft Matter Physics
Institute for Experimental Physics
Johannes Kepler University
Altenberger Str. 69, Linz 4040, Austria
E-mail: martin.kaltenbrunner@jku.at
F. Hartmann, L. Penkner, D. Danninger, Dr. N. Arnold,
Prof. M. Kaltenbrunner
Soft Materials Lab
Linz Institute of Technology
Johannes Kepler University
Altenberger Str. 69 Linz 4040, Austria

of an optical system with a single tunable lens represents a frugal approach with versatile potential applications, including vision systems for soft robotics, humanoids, or highly miniaturized optical systems.[3,4]

Typically, tunable lenses take advantage of deformable lens-shaped liquids, elastomers, or liquid-filled elastic membranes, which change their focus with the help of electroactive transducers or materials. Commercially available lenses—based on electrowetting or reshaping rings—have liquid or soft optical components but require rigid encapsulations and actuators, which partially negate the advantages of soft materials.[5,6] Tunable lenses with micro-pumps achieve high image quality with little aberrations, yet at the cost of size and compactness.[7–9] Approaches utilizing inhomogeneous electric fields to reshape lens droplets potentially minimize the usage of rigid parts, but exhibit slow response times typically of the order of seconds.[10,11] Similarly, stimulus-responsive soft materials such as hydrogels exhibit response times of tens of seconds as they are based on water diffusion or changing environments.[12] Lenses tuned by dielectric elastomer actuators (DEAs) overcome all these limitations, as they operate at high speeds, are electrically driven and soft.[1,13–15] Such lens-actuator systems closely mimic designs found in nature as the contraction of DEAs resembles ciliary muscles deforming the lens in the human eye.[16] Their compactness and speed renders DEAs useful for such artificial (ciliary) muscles, with advantages over pneumatic actuators, thermally driven shape memory alloys or magnetically driven soft actuators, which usually require pumps, external heat sources or external magnetic fields.[17,18] Yet, DEAs require high driving voltages in the kilovolts range and suffer from dielectric breakdowns, which irreversibly damage the lens (Table S1, Supporting Information). Actuators based on the displacement of dielectric liquids via zipping electroactive polymers (ZEAP) survive dielectric breakdown and have promising applications as artificial muscles for soft robotics[19,20] and wearable haptic displays,[21] but they require high driving voltages as well.

Here we introduce broadly applicable design rules, analytical models, and fabrication methods for soft tunable lenses based on ZEAP actuators operating at practical voltages. Zipping of thin metal-coated plastic foils induces a hydraulic volume transfer, leading to shape change of elastic membranes at voltages

Figure 1. Tunable soft lenses with ZEAP actuators. a) Schematic of the tunable soft lens. Zipping of the actuator electrodes inflates the lens membrane in the center. b) In the off-state the lens membrane is nearly flat and the dielectric liquid is evenly distributed. c) In the on-state the metalized plastic foils contract due to the applied electric field, which inflates the lens membrane and magnifies the image (the letter "M"). d) Lens 3-mm-aperture radius and small actuator (16 mm diameter). e) Lens 3-mm-aperture radius and large actuator (30 mm diameter). The patterned electrodes aid concentric actuation.

below 500 V and focal length changes from 550 mm to as low as 22 mm, which equals a change of 0.005–0.14 in numerical aperture. The ZEAP actuators autonomously self-heal from dielectric breakdown and allow fast focal length changes within milliseconds. Analytic and numerical models allow optimized designs and prediction of lens performances that agree well with the experiments. Our first results demonstrate powerful new types of soft tunable lenses for soft machines and robotics that are easily scalable, low-cost, and allow for large focal length changes.

Our tunable lens architecture consists of a deformable elastomeric membrane in the center, circumvented by a circular ZEAP actuator (**Figure 1**a). The membrane and the actuator share a reservoir of dielectric oil, which is radially injected toward the center when the polymer foils of the actuator zip, thus inflating the membrane. ZEAP actuators are built as metal-insulator-metal structures that use a dielectric liquid as insulator. In the off-state, the dielectric liquid separates two metalized polymer foils—we here use 6-µm thick polyethylene terephthalate (PET) metalized with 150 nm copper (Cu)—in balance with the lens membrane at its initial curvature (Figure 1b). Applying a voltage induces an electric field between the electrodes, which contract and start to zip, displacing the dielectric liquid. As the lens membrane has a low elastic modulus and thickness, it is inflated, resulting in a decreasing focal length and larger image magnification (Figure 1c). While the dielectric liquid is the main insulator in the off-state, the polymer foil separates the metal electrodes when the actuator is zipped. Its thickness, permittivity, and initial opening angle mainly determine the operating voltage of the tunable lens. Here, we use an asymmetric electrode orientation to reduce the zipped capacitor thickness and operating voltage; the metallization of the PET-foils faces downward for both electrodes (Cu-PET-Cu-PET instead of the typically used Cu-PET-PET-Cu). The size of the actuator determines the maximum amount of displaceable liquid and is readily adjusted without changing the fabrication methods (Figure 1d,e).

As the lens performance depends on various design parameters such as membrane thickness and actuator dimensions, we modeled the lenses analytically and numerically to predict the focus versus voltage characteristics. The calculation is based on minimization of the system free energy $W(\Delta V)$, which separates into a load-term, describing the elastic energy of the lens membrane, and an actuator-term, representing the electrical energy in terms of voltage U and total capacitance C (details on the geometry are given in Figure S1 and Table S2, Supporting Information).

$$W = \int_{0}^{V_0 + \Delta V} p(V)\,dV - C(\Delta V)\frac{U^2}{2}$$
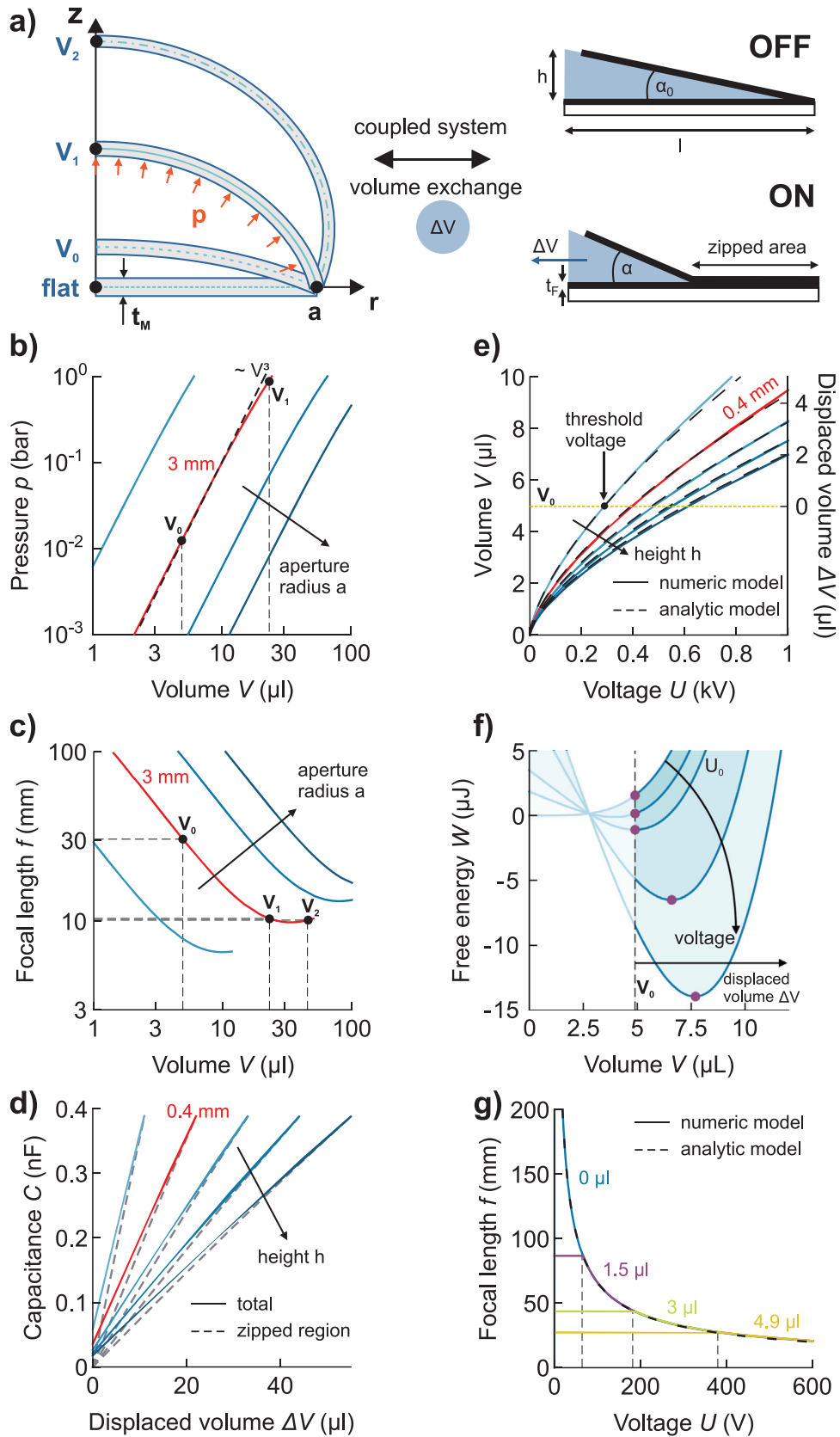
The first term here is elastic in nature, but it can be conveniently recalculated from the work–energy balance during the inflation, while the sign of the second term is negative under the voltage-controlled conditions due to the work of the battery.[22,23] These two terms are coupled by the amount of displaced (incompressible) dielectric liquid $\Delta V = V - V_0$, which inflates the membrane starting from an initial state (off-state) with volume V_0 to volume V (voltage dependent on-state) (**Figure 2**a). Our analytic models approximate the membrane shape as a spherical cap, inflated by low amounts of displaced volume. This results in power laws for the pressure–volume (p–V) and focal-length–volume (f–V) characteristics. For the numerical models, we use a system of ordinary differential equations with boundary conditions, based on a previous work,[24] to describe the membrane shape and p–V characteristic. The paraxial focus is then obtained numerically from the membrane shape, applying Snell's law (for details, see Discussion in Supporting Information). Both analytic and numeric p–V characteristics result in power laws with exponent 3, with minor deviations at larger volumes (Figure 2b). An increasing aperture reduces energy required for a fixed volume change (given by the $\int p dV$), and defines the working range of the tunable lenses.

Inflation of the membrane decreases the focal length following a power law with exponent -1 in the working regime between V_0 and V_1 (Figure 2c). Beyond this range, further displaced volume results in overall membrane stretch only, with little curvature changes around the apex.

The actuator, in electrical terms a simple capacitor, delivers the energy required to inflate the membrane. Its capacitance C, with contributions from the zipped and unzipped region, almost linearly changes with displaced volume (Figure 2d). Previous calculations for Peano-HASEL actuators (a special form of uniaxial ZEAP actuators) assume that the capacitance is mostly determined by the zipped region alone.[25] While this assumption gives a good approximation for large actuator heights h (hence large opening angles of the electrodes), the contribution of the unzipped region increases for small heights and cannot be neglected near the fully unzipped state. In a general description, the minimization of free energy (1) with respect to displaced volume ΔV (internal variable of the system) results in force balance for any ZEAP tunable lens, which can be written as:

$$p\left(V_0 + \Delta V\right) = \frac{dC}{d\Delta V}\frac{U^2}{2}$$

Here, U is the applied voltage. This equation relates the applied voltage to the displaced volume with good agreement for both numerical and analytic approaches (Figure 2e). The final focal-length–voltage char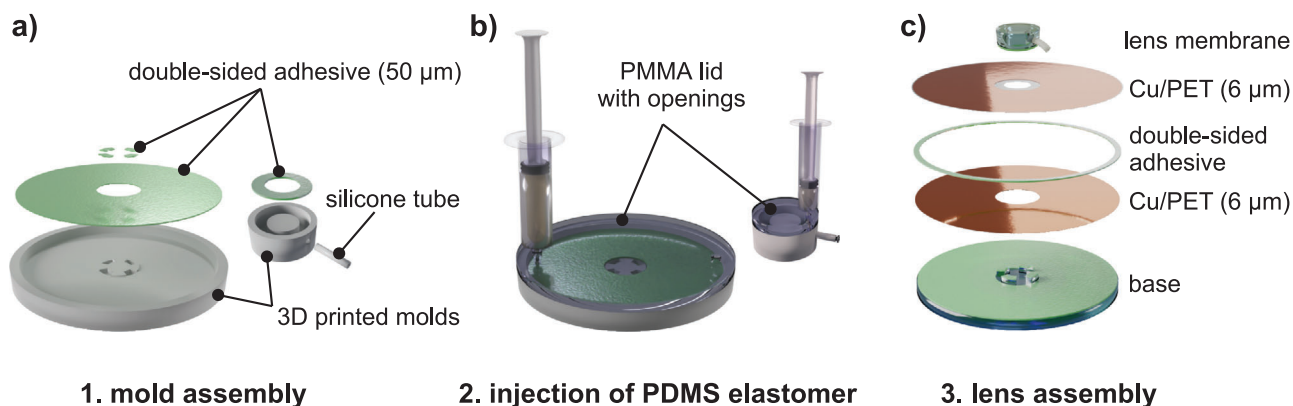acteristic $f(U)$ is then obtained recalculating the volume V into focal length f for a given geometry, resulting in:

$$f\left(U\right) = \frac{\pi a}{4\left(n - 1\right)}\left(\frac{U_c}{U}\right)^{2/3}$$

Here, U_c is the characteristic voltage, which includes the majority of material and design parameters except basic scaling with aperture size a, refractive index n, and V_0, and is a quantity that relates to the operating voltage (see Discussion in Supporting Information). An essential feature of the system is the emergence of a critical (threshold) voltage $U_0 = (V_0/a^3)^{3/2} U_c$, below which no changes take place. The free energy has a minimum at $V > V_0$ only if U surpasses this threshold voltage (Figure 2f). Both the initial focal length f_0 and threshold voltage U_0 are determined by the initial filling volume V_0, which limits f from above. The threshold vanishes for $V_0 = 0$ (no filling volume), where f_0 becomes infinite. For lenses with 3-mm aperture radius and a 200-µm-thick membrane, the focal length is readily tuned with voltages below 500 V and threshold voltages are below 200 V for initial fillings up to 3 µL (Figure 2g).

Design of sub-kV tunable lenses with high range of focal length changes is based on guidelines from our models, while choosing inexpensive commodity materials. Our theoretical analysis provides design routes that yield even lower operating voltages (<100 V) and are outlined in the Supporting Information. The fabrication starts with thermal evaporation of 150 nm Cu on 6 µm thick PET-foil. Where no electrodes are needed, Cu is removed with laser-induced ablation, and the PET-foil is subsequently cut in shape by laser machining. A bottom elastomer base for structural support and the lens membrane are mold-cast from polydimethylsiloxane (PDMS) using 3D printed molds with polymethyl methacrylate (PMMA) covers (**Figure 3**a,b). This results in an overall soft structure that is compressible and flexible (Figure S2, Supporting Information). Double-sided 50-µm-thick elastic adhesion tape connects the individual parts of the lens, which are readily stacked on top of each other (Figure 3c). The connection of lens membrane and base keeps the membrane in a fixed position and allows homogenous inflation (and pressure) by the dielectric fluid. Omitting this connection can lead to directional inflation of the membrane, which is beneficial for other applications that involve touch, such as buttons or brail displays.[21] Heat-sealing the electrodes in regular steps along the edge of the electrodes introduces specific starting points for zipping to improve the zipping homogeneity (we use this for all our lenses) and partially reduces the threshold voltage (Figure S3, Supporting Information). The dielectric fluid is a low viscosity paraffin oil with a refractive index $n = 1.48$ (close to PDMS); it is

Figure 2. Modeling of soft tunable lenses. a) Applying a voltage to the actuator electrodes leads to a zipping induced volume exchange inflating the lens membrane ($t_M = 0.2$ mm, no pre-stretch), which deforms from $V_0 = 4.9$ µL to $V_1 = 23$ µL and $V_2 = 45$ µL. b) Pressure–volume characteristics follow a power law in the working range between V_0 and V_1. c) Focal-length–volume characteristics for membranes with different aperture radii (2, 3, 4, and 5 mm, additional design parameters are fixed). Volumes larger than V_1 have minor influence on the focal length. d) The capacitance of the electrodes is nearly linear in displaced volume, with dominant contribution from the zipped region. Characteristics are calculated for different actuator heights (0.2, 0.4, 0.6, 0.8, 1 mm, additional design parameters are fixed). e) The balance of mechanical and electrical forces yields the volume–voltage relations for different actuator heights. Initial fillings V_0 lead to a threshold voltage that is required to displace volume from actuator to the lens membrane. f) The free energy of the system with boundary condition V_0 exhibits a minimum at $V > V_0$ when a voltage greater the threshold voltage (U_0) is applied. g) Combining the results from (c) and (e) leads to the focal-length–voltage characteristics for different initial volumes (0, 1.5, 3, 4.9 µL) and respective threshold voltages.

ADVANCED
SCIENCE NEWS

www.advancedsciencenews.com

ADVANCED
SCIENCE
Open Access

www.advancedscience.com

Figure 3. Soft lens fabrication and assembly. a) 3D printed molds for the lens membrane and base. Double-sided adhesive is loosely applied within the molds to allow easy lens assembly. b) Molds are covered with PMMA lids, and PDMS elastomer is injected through one of the access holes. c) The lens is assembled together with the actuator electrodes using adhesive tape and filled with paraffin oil through the attached silicon tube.

injected with a syringe through an access tube and sealed. Lenses with a larger actuator are produced without changing the fabrication methods but require—in addition to heat-seals— structuring of the electrodes to achieve more homogeneous zipping (Figure S4, Supporting Information). We realize this by engraving concentric rings into the electrodes, which results in ring-by-ring zipping and nearly concentric zipping fronts (Figure S5, Supporting Information). The total material costs for a single lens are about 14 cents and are majorly (96%) dominated by the PDMS elastomer (see Discussion and Table S3 in Supporting Information).

For a 3-mm aperture radius lens, an actuator with 16 mm diameter is sufficient to inflate the lens membrane to full extent (maximum focal length change). Depending on the filling level, the initial focal length is freely adjusted; here we present three lenses with ≈50, 110, and 550 mm initial focal length (**Figure 4**a–c and Figure S6, Supporting Information). According to the models, the focal length remains constant below the threshold voltage, which decreases for smaller initial fillings (larger maximal focal length). However, the experimental behavior below and near the threshold is influenced by locally varying zipping, caused by the heat seals or other inhomogeneities (Figure 4a–c). A voltage of 450 V reduces the focal length to about 22 mm for all lenses, in agreement with our models. Deviations from the model occur in the mid-voltage range (100–200 V) for the lens with the largest initial focal length (Figure 4c). We hypothesize that lower initial fillings lead to less uniform opening angles of the electrodes and less concentric zipping. This effect is also visible for the lenses with large actuators, which feature smaller electrode opening angles and therefore potentially lower operating voltages (Figure S7, Supporting Information), albeit with a less ideal zipping behavior.

The dynamic performance of the lenses is tested by deflecting a laser beam passing slightly off the optical axis (Figure 4d, Figure S8, Supporting Information). The relative change of the tangent of the beam angle with the optical axis, or the relative laser spot position at any image plane, is proportional to the relative focal length change (see Discussion in Supporting Information). Applying a step function with 2 s pulse width and 600 V amplitude visualizes the rates for switching lenses from the on- to the off-state, averaged over 100 switching cycles (Figure 4e). The switching to the on-state is faster; it requires about 260 ms to reach about 95% of the maximal focal length change. Once switched on, the lens retains its focus for the duration of the pulse. When switched off, it takes about 500 ms to return to within 15% change from the initial focal length change. This performance is comparable to a young human eye (20–30 y), which achieves 240 ms reaction time for near accommodation.[26] Switching to the on state is inherently faster, since this process is electrically driven by the actuator, while switching to the off state is a passive process governed by the mechanic relaxation of the system. The frequency-dependent performance of the lenses is tested by applying triangular waves with 400 V amplitude at different frequencies. We quantify the performance by the fraction of the beam deflection to its maximum possible value $\Delta\gamma/\Delta\gamma_{max}$, and define the performance at 1 Hz as 100%. Increasing the frequency decreases the lenses performance, which however remains above 25% at 10 Hz (Figure 4f). The relative deflection of the laser beam shows little hysteresis during 100 repeated actuation cycles actuation with 1 Hz, yet a slight drift is visible, which however stabilizes after a few 100 cycles (Figure 4g, Figure S9, Supporting Information). Enhanced lens control can be achieved using the capacitance— capacitance and displaced volume relate nearly linearly—as additional control parameter in a closed-loop[27] and provides a possible solution to compensate drifts.

We report a versatile strategy to fabricate entirely soft electrically tunable lenses that operate at voltages below 500 V. Analytic and numerical models that describe the combined deformable lens-actuator system are presented, which can be applied to a wide range of ZEAP-actuated systems. The focal length can be rapidly changed between 550 and 22 mm within milliseconds. With the current design and materials, the lens maintains 25% of its performance even at switching speeds as high as 10 Hz. Even faster actuation speeds are possible by choosing dielectric liquids with lower viscosity, and optimizing the fluidic channels within the lens. Usage of plastic foils with either lower thickness or higher permittivity further reduces the operating voltages. Our approach represents a major step towards low-voltage electroactive actuators, applicable to tunable optics, soft machines and robotics.
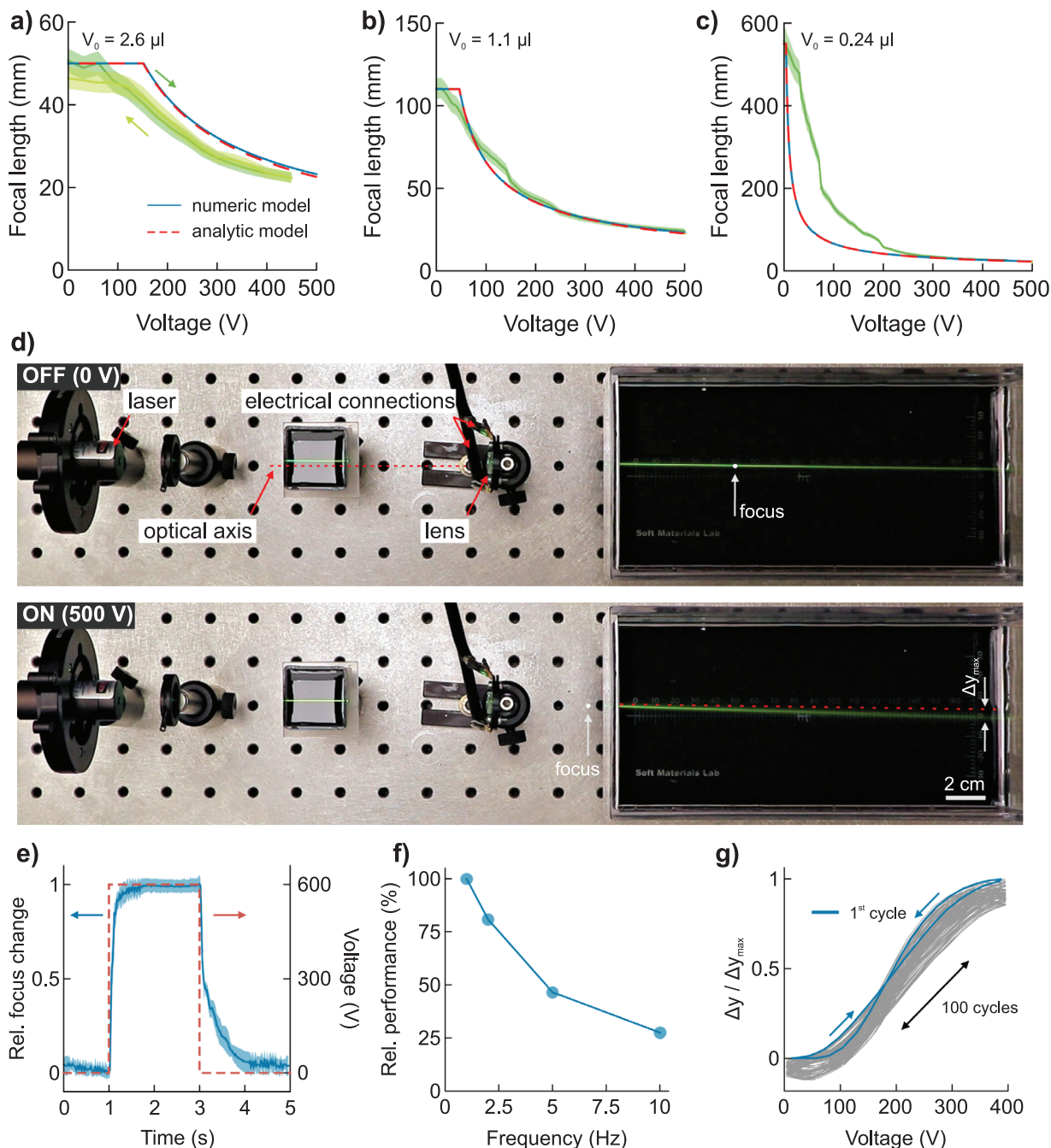
Figure 4. Lens performance. a–c) Measured focal-length–voltage characteristics in comparison to numerical (blue) and analytic models (red dashed) for lenses with different initial focal lengths. d) Laser beam deflection through the tunable lens during operation. The maximum deflection is denoted as Δy_{max}. e) Response to step signal with 600 V amplitude is averaged over 100 cycles and results in 260 ms to reach 95% rel. focus change. Error band, standard deviation for 100 cycles. f) Relative performance as a function of frequency for triangular wave driving voltages with 400 V amplitude. g) Relative deflection change for 100 continuous actuation cycles.

Experimental Section

Materials: All chemicals were used as received without further purification. Polydimethylsiloxane, PDMS (Sylgard 184, Dow-Corning, USA) was used for the lens body and membrane. Dow-Corning Primer (DOWSIL 1200 OS Primer, Dow-Corning, USA) and acrylic elastomer adhesive tape (VHB 467MP, 3M, USA) were used to bond PDMS to the PET foils of the

actuator. Paraffin oil (Paraffin oil thin, Roth, Germany) was used as a liquid dielectric.

Base and Membrane Fabrication: High precision molds were 3D printed with a stereolithography printer (Form 3, Formlabs, USA) and post-cured at 60 °C under UV light. VHB adhesive tapes were laser cut (Speedy 300 flexx, Trotec, Austria), coated with a thin layer of primer using an airbrush gun, and fixed within the molds. The molds were closed with PMMA

covers, which feature two access holes for polymer injection. The membrane molds additionally feature a lateral hole, where a small silicon tube was mounted and sealed. PDMS prepolymer and cross-linker were mixed 10:1 in a planetary mixer (SpeedMixer DAC400, Hausschild, Germany) under vacuum, injected into the molds with a syringe, and cured at 65 °C for at least 6 h.

Electrodes Fabrication: 150 nm Cu was thermally evaporated (Univex350, Leybold, Germany) on 6-µm thin PET foil, with 3 nm of chromium as adhesion layer. The electrodes were structured using laser ablation and laser cut into the desired shapes.

Lens Assembly: Base, electrodes, and lens membrane were stacked together utilizing the cast-in adhesives, with an additional ring of VHB between the two electrodes. Spot welding was used for all lenses to introduce starting points for zipping fronts. Therefore, the electrodes were covered with 75-µm-thick polyimide and the 185 °C-hot nozzle of a 3D printer (Ultimaker 3, Ultimaker, Netherlands) was used for welding (10 s). All lenses were filled and vented with paraffin oil via the silicon tube and sealed in advance.

Focal Length Measurement: The lens was placed under an objective (8×) of a microscope (Micromanipulator, model 6200), equipped with a digital camera (Bresser, MikroCam SP 5.0). A micrometer scale served as image to measure the magnification, from which the focal length was calculated. A function generator (33250A, Agilent Technologies, USA) and a voltage amplifier (PD05034, Trek Inc., USA) drove the lens, applying a 50 Hz bipolar square wave signal with voltages up to ±450 V.

Response Characterization: A laser beam (wavelength 450 nm) with slight offset to the optical axis was directed through the lens and basins filled with water-diluted rhodamine 6 g. The lens was driven with a voltage amplifier, which was controlled by a function generator. A step function of 2 s pulse width (5 s period) and 600 V amplitude was applied to investigate the response behavior. For dynamic characterization a 400 V (1–10 Hz) triangular wave signal was applied. The experiments were recorded at 50 fps with a camera and evaluated via beam tracing.

Supporting Information

Supporting Information is available from the Wiley Online Library or from the author.

Acknowledgements

Conflict of Interest

The authors declare no conflict of interest.

Author Contribution

F.H. and M.K. conceived the research project; N.A., F.H., and L.P. derived analytic and numerical models; L.P. and F.H. designed and fabricated the tunable lenses; F.H. and L.P. designed the experiments; L.P. conducted the characterizations; F.H., L.P., and D.D. prepared the figures and tables; F.H., L.P., D.D., and N.A. wrote the manuscript; all authors contributed to editing the manuscript; F.H. and M.K. supervised the research.

[1] F. Carpi, G. Frediani, S. Turco, R. D. De, *Adv. Funct. Mater.* **2011**, *21*, 4152.

[2] J. J. Kim, H. Liu, A. Ousati Ashtiani, H. Jiang, *Rep. Prog. Phys.* **2020**, *83*, 047101.

[3] S. Petsch, S. Schuhladen, L. Dreesen, H. Zappe, *Light: Sci. Appl.* **2016**, *5*, 16068.

[4] G. J. Lee, C. Choi, D. H. Kim, Y. M. Song, *Adv. Funct. Mater.* **2018**, *28*, 1705202.

[5] "Corning Inc.," can be found under https://www.corning.com/worldwide/en/innovation/corning-emerging-innovations/corning-varioptic-lenses.html, **n.d.**

[6] "Optotune Switzerland AG," can be found under https://www.optotune.com/tunable-lenses, **n.d.**

[7] L. Li, Q. H. Wang, W. Jiang, *J. Opt.* **2011**, *13*, 115503.

[8] L. Wang, H. Oku, M. Ishikawa, *Appl. Phys. Lett.* **2013**, *102*, 131111.

[9] P. Zhao, C. Ataman, H. Zappe, in *Proc. IEEE Int. Conf. Micro Electro Mech. Syst.*, IEEE, Shanghai, China **2016**.

[10] M. Xu, D. Xu, H. Ren, I. S. Yoo, Q. H. Wang, *J. Opt. (Bristol, U. K.)* **2014**, *16*, 105601.

[11] B. Jin, H. Ren, W.-K. Choi, *Opt. Express* **2017**, *25*, 32411.

[12] L. Dong, A. K. Agarwal, D. J. Beebe, H. Jiang, *Nature* **2006**, *442*, 551.

[13] D. Wirthl, R. Pichler, M. Drack, G. Kettlguber, R. Moser, R. Gerstmayr, F. Hartmann, E. Bradt, R. Kaltseis, C. M. Siket, S. E. Schausberger, S. Hild, S. Bauer, M. Kaltenbrunner, *Sci. Adv.* **2017**, *3*, 1700053.

[14] L. Maffli, S. Rosset, M. Ghilardi, F. Carpi, H. Shea, *Adv. Funct. Mater.* **2015**, *25*, 1656.

[15] S. Shian, R. M. Diebold, D. R. Clarke, *Opt. Express* **2013**, *21*, 8669.

[16] S. Nam, S. Yun, J. W. Yoon, S. Park, S. K. Park, S. Mun, B. Park, K. U. Kyung, *Soft Rob.* **2018**, *5*, 777.

[17] S. M. Mirvakili, I. W. Hunter, *Adv. Mater.* **2018**, *30*, 1704407.

[18] G. Mao, M. Drack, M. Karami-Mosammam, D. Wirthl, T. Stockinger, R. Schwödiauer, M. Kaltenbrunner, *Sci. Adv.* **2020**, *6*, 0251.

[19] N. Kellaris, V. G. Venkata, G. M. Smith, S. K. Mitchell, C. Keplinger, *Sci. Rob.* **2018**, *3*, 3276.

[20] X. Cheng, M. Yu, J. Ma, B. Li, Y. Zhang, P. Wang, Z. Jiao, *Smart Mater. Struct.* **2020**, *29*, 045017.

[21] E. Leroy, R. Hinchet, H. Shea, *Adv. Mater.* **2020**, *32*, 2002564.

[22] C. Keplinger, M. Kaltenbrunner, N. Arnold, S. Bauer, *Proc. Natl. Acad. Sci. U. S. A.* **2010**, *107*, 4505.

[23] Z. Suo, *Acta Mech. Solida Sin.* **2010**, *23*, 549.

[24] P. Pokorný, F. Šmejkal, P. Kulmon, P. Novák, J. Novák, A. Mikš, M. Horák, M. Jirásek, *Appl. Opt.* **2017**, *56*, 9368.

[25] N. Kellaris, V. G. Venkata, P. Rothemund, C. Keplinger, *Extreme Mech. Lett.* **2019**, *29*, 100449.

[26] T. E. Lockhart, W. Shi, *Ergonomics* **2010**, *53*, 892.

[27] K. Ly, N. Kellaris, D. McMorris, B. K. Johnson, E. Acome, V. Sundaram, M. Naris, J. S. Humbert, M. E. Rentschler, C. Keplinger, N. Correll, *Soft Robotics* **2020**, https://doi.org/10.1089/soro.2020.0048.

Supporting Information

Soft tunable lenses based on zipping electroactive polymer actuators

Florian Hartmann, Lukas Penkner, Doris Danninger, Nikita Arnold, and Martin Kaltenbrunner

Supplementary Information

Soft tunable lenses based on zipping electroactive polymer actuators.

Florian Hartmann[1,2], Lukas Penkner[1,2], Doris Danninger[1,2], Nikita Arnold[1,2], and Martin Kaltenbrunner[1,2]

[1]Division of Soft Matter Physics, Institute for Experimental Physics, Johannes Kepler University Linz, Altenberger Strasse 69, 4040 Linz, Austria
[2]Soft Materials Lab, Linz Institute of Technology, Johannes Kepler University Linz, Altenberger Strasse 69, 4040 Linz, Austria

Correspondence to: martin.kaltenbrunner@jku.at

This PDF file includes:

Supplementary Discussion

Supplementary Tables 1-3

Supplementary Figures 1-9

Supplementary Discussion

Total free energy of a tunable soft lens with actuator

The (free) energy W of the whole tunable lens system splits into the energy of the lens membrane W_M and the energy of the actuator W_A.

$$W = W_M + W_A \tag{1}$$

In a quasi-static description, which we assume to suffice for moderate operating speeds, we neglect dynamic effects, such as kinetic energy and the acceleration of the dielectric liquid and the ambient medium (air in our case). Strategies for analysis of dynamic effects can be found in the literature [1,2]. The elastic energy of the membrane resides in the stretched elastomer, but it can be calculated from the integral of its pressure-volume (p-V) characteristic, where the initial filling level V_0 defines the reference state. In this reference state, no voltage is applied, and the actuator/lens membrane system is in balance, due to equilibrium between the over-pressure and elasticity. In the actuated state, the electrodes of the actuator are connected to a constant voltage source, which then zip, and inflate the lens membrane to filling levels $V > V_0$. The difference in volume $\Delta V = V - V_0$ is called displaced volume, it is the volume exchanged between the actuator and lens membrane. We consider only reference states with convex lens shapes, hence $V_0 \geq 0$, however states with $V_0 < 0$ can be experimentally realized and modelled within our framework. We calculate the elastic (free) energy of the incompressible lens membrane as

$$W_M = \int_0^{V_0 + \Delta V} p(V)\,\mathrm{d}V \tag{2}$$

To derive the actuator energy W_A, we model the actuator as a radial-symmetric capacitor, surrounding the lens membrane. Its capacitance $C(\Delta V)$ changes, as the actuator zips. W_A is dominated by the electrostatic contributions; the elastic energy of the actuator is much smaller than for the lens membrane, because the product of its material stiffness and thickness is one order of magnitude larger. The electrostatic energy of the capacitor $W_{A'}$ is:

$$W_{A'} = \frac{Q^2}{2C} \tag{3}$$

As the actuator zips, its capacitance increases, and the charges are provided by the power supply with the constant voltage U. The work of the external power supply QU should be subtracted in the energy balance, which reverses the sign of the electrostatic contribution to *free* energy [3,4], which then becomes:

$$W_A = -\frac{CU^2}{2} \tag{4}$$

The total free energy of the system (up to an arbitrary constant) is then written as[1]

$$W = \int_0^{V_0 + \Delta V} p(V)\,\mathrm{d}V - \frac{U^2}{2}C(\Delta V) \tag{5}$$

The equilibrium condition is provided by the minimum of this expression with respect to the internal system variable ΔV, resulting in

$$p(V_0 + \Delta V) = \frac{U^2}{2}\frac{d\,C(\Delta V)}{d\Delta V} \tag{6}$$

In the next sections, we derive expressions for $p(V)$ and $C(\Delta V)$ and provide an analytical model for the focus-voltage characteristics of ZEAP tunable lenses.

---

[1]The *elastic* energy of the dielectric fluid can be neglected, as it is considered to be incompressible. Its compression response is much stiffer, than the elastic response of the membrane, which defines the lens volume. Under such conditions, all the elastic energy is stored in the softer material.

Inflation of a planar elastomer-membrane with prestretch

Consider a thin circular elastic membrane with initial radius a and *relaxed, unstretched* thickness t_{M}, which is clamped along its circumference, and is inflated by a uniform pressure p. The z-axis is the symmetry axis and r is the polar radius. In general case, the membrane can have an initial lateral equal-biaxial prestretch λ_0. The height of the inflated membrane in z-direction is denoted as Z^2, its area as S, and the enclosed volume as V.

Assuming that the inflated membrane is a spherical cap, these quantities can be written as

$$S = \pi \left(a^2 + Z^2\right) = \pi \frac{a^2 \lambda^2}{\lambda_0^2} \tag{7}$$

$$V = \frac{\pi h}{6} \left(3a^2 + Z^2\right) = \frac{\pi a^3}{6} \left(2 + \frac{\lambda^2}{\lambda_0^2}\right) \sqrt{\frac{\lambda^2}{\lambda_0^2} - 1} \tag{8}$$

Here, λ is the average stretch, based on the area change with respect to its initial value (which may includes a prestretch λ_0). From eq. (7) we obtain:

$$\lambda = \lambda_0 \sqrt{1 + Z^2/a^2} \tag{9}$$

Using the work-energy balance $p\mathrm{d}V = V_{\mathrm{M}}\mathrm{d}G$, where V_{M} is the (constant) volume of the (thin, incompressible) membrane, we can relate the (over)pressure to the derivative of the elastic energy density G_λ

$$p = V_{\mathrm{M}} \frac{\mathrm{d}G}{\mathrm{d}V} = \frac{\pi a^2 t_{\mathrm{M}}}{\lambda_0^2} \frac{G_\lambda}{\mathrm{d}V/\mathrm{d}\lambda} = \frac{2\lambda_0 \sqrt{\lambda^2 - \lambda_0^2}}{\lambda^3} \frac{t_{\mathrm{M}}}{a} G_\lambda \tag{10}$$

The expression (10) is rather general.[3] The $p(V)$ dependence can be simplified for small stretches without prestretch, where the Neo-Hookean relation holds for G and $\lambda = 1 + \delta\lambda$, $\delta\lambda \ll 1$. This case is the most relevant for elastomer lens modelling. With the shear modulus μ, the derivative of elastic energy density is written as

$$G_\lambda = 2\mu \left(\lambda - \lambda^{-5}\right) \approx 12\mu \, \delta\lambda \tag{11}$$

This results in simplified expressions for the pressure, while the volume can be obtained from the eq. (8)

$$p \approx 24\sqrt{2} \, \frac{\mu \, t_{\mathrm{M}}}{a} \delta\lambda^{3/2} \tag{12}$$

$$V \approx \pi a^3 \sqrt{\frac{\delta\lambda}{2}} \tag{13}$$

Combining both equations results in the pressure-volume characteristics for the initial stage.

$$p(V) = \frac{3 \times 2^5}{\pi^3} \frac{\mu \, t_{\mathrm{M}}}{a} \left(\frac{V}{a^3}\right)^3 \tag{14}$$

This approximations assumes small homogeneous stretch.[4] In reality, the stretch and membrane thickness vary along the membrane, and its shape deviates from a spherical cap. A more accurate

---

[2]It is often convenient to use Z as an underlying parametrizing variable instead of V or λ, especially in the intermediate calculations.

[3]It is instructive to compare it with the similar result for a spherical balloon with initial unstretched radius a, $p = t_{\mathrm{M}} G_\lambda / a\lambda^2$.

[4]With prestretch, the dependence (14) changes drastically, and becomes linear in volume V. This may be used for better control of the system, but requires more rigid design parts, which we aimed to avoid in this work.

fast calculation for the p-V-characteristic can still be performed numerically within the frame of linear material elasticity.[5]

Numeric calculations for the inflation of a circular elastic membrane are based on a model from Pokorny *et al.* [5]. The applied pressure deforms the membrane such, that a point with initial coordinates $(r, 0)$ moves to the position $(r + u(r), w(r))$ (Supplementary Fig. S2). Thus, $u(r)$ and $w(r)$ represent the radial displacement and the deflection in z-direction. An initial prestretch λ_0 of the membrane causes a radial stretch λ_r and a tangential stretch λ_t in the deformed state, expressed as

$$\lambda_r = \lambda_0 \sqrt{(1 + u'(r))^2 + w'(r)^2} \tag{15}$$

$$\lambda_t = \lambda_0 \left(1 + \frac{u(r)}{r}\right) \tag{16}$$

where $u'(r)$ and $w'(r)$ are the derivatives with respect to r. For a linear Saint Venant-Kirchhoff material, these stretches define the radial, tangential and initial stress, σ_r, σ_t and σ_0 respectively, via Young's modulus E and Poisson ratio ν.

$$\sigma_r = \frac{E \lambda_0^2}{2(1 - \nu^2)} \left(\left(\frac{\lambda_r^2}{\lambda_0^2} - 1\right) + \nu \left(\frac{\lambda_t^2}{\lambda_0^2} - 1\right)\right) + \sigma_0 \tag{17}$$

$$\sigma_t = \frac{E \lambda_0^2}{2(1 - \nu^2)} \left(\left(\frac{\lambda_t^2}{\lambda_0^2} - 1\right) + \nu \left(\frac{\lambda_r^2}{\lambda_0^2} - 1\right)\right) + \sigma_0 \tag{18}$$

$$\sigma_0 = \frac{E (\lambda_0^2 - 1)}{2(1 - \nu)} \tag{19}$$

The stresses and shape of the elastomer membrane are given by a system of ordinary differential equations

$$\frac{\partial}{\partial r} \left(r \sigma_r (1 + u'(r))\right) - \sigma_t \left(1 + \frac{u(r)}{r}\right) = \frac{p}{t_M} w'(r) (u(r) + r) \tag{20}$$

$$-\frac{\partial}{\partial r} \left(r \sigma_r w'(r)\right) = \frac{p}{t_M} (u'(r) + 1) (u(r) + r) \tag{21}$$

with the boundary conditions

$$w'(0) = 0$$
$$w(a) = 0$$
$$u(0) = 0$$
$$u(a) = 0$$

For numerical calculations we use small values (e.g. 10^{-4}) for all dimensionless zero values, to avoid singularities. Solving these equations for different applied pressures gives the respective membrane shapes and enclosed volumes, resulting in the required pressure-volume characteristics, which can be used in further analysis. In particular, the paraxial focal length of the inflated membrane is calculated from the membrane shape[6].

Capacitance of a radially-symmetric electrostatic zipping actuator

To derive the electrostatic actuator energy W_A, an expression for the capacitance C is required. The actuator consists of a fixed bottom electrode with inner radius c and outer radius $c + l$ (radial length

---

[5]The *geometrical* nonlinearities are taken into account in this approach

[6]We calculate the focal length by ray tracing of parallel rays applying Snell's law. Rays within $10^{-2}a$ from the optical axis are considered and averaged.

l), and a top electrode with small slope (Supplementary Fig. S2). The initial opening angle between top and bottom electrode α_0 and is given by the actuator height h and length l.

$$h = l \tan \alpha_0 \tag{22}$$

When voltage is applied, the top electrode collapses from the outer edge, resulting in a zipped region with the radial length l_1 (and $l_L = l - l_1$ for the unzipped region), and the opening angle changes to α. The capacitance of the actuator is the sum of the capacitance of the zipped region C_1 and of the unzipped region C_L.[7]

$$C = \underbrace{\frac{\varepsilon_F S_1}{t_F}}_{\text{zipped } C_1} + \underbrace{\int \frac{\varepsilon_F \varepsilon_L}{\varepsilon_L t_F + \varepsilon_F t_L(r)} \, dS_L}_{\text{unzipped } C_L} \tag{23}$$

Here, S_1 is the area of the zipped region, S_L the area of the unzipped region, ε_F the permittivity of the plastic foil with thickness t_F, and ε_L the permittivity of the dielectric liquid with the radially changing thickness $t_L(r)$. The first term describes the capacitance of the zipped region C_1 and can be expressed as a function of the displaced volume.

$$C_1(\Delta V) = \frac{\pi \varepsilon_F}{t_F} \, l_1(\Delta V) \left(2(c+l) - l_1(\Delta V)\right) \tag{24}$$

Assuming linear thickness dependence on radius $t_L(r)$ (cone-shaped actuator), the integration in eq. (23) results in the capacitance of the unzipped region, which can be conveniently expressed via its outer radius $R = c + l - l_1$

$$C_L = \frac{2\pi \varepsilon_L l_L^2}{h} \left(\left(\frac{R}{l_L} + \frac{\varepsilon_L t_F}{\varepsilon_F h} \right) \ln \left(1 + \frac{\varepsilon_F h}{\varepsilon_L t_F} \right) - 1 \right) \tag{25}$$

The capacitance ratio C_L/C_1 is large for small zipping regions with $l_1 << l_L$. For a typical zipping regions with $l_1 \sim l_L$ and $\varepsilon_L \sim \varepsilon_F$ this ratio is of the order of

$$\frac{C_L}{C_1} \sim \frac{t_F}{h} \ln \left(\frac{h}{t_F} \right) \tag{26}$$

This ratio is small only asymptotically (for thin films with $t_F << h$), and is often ~ 1 for typical numbers. However, for the *derivatives* with respect to ΔV (which enter the expression (6) for the pressure), $C_L'(\Delta V)$ is usually much smaller than $C_1'(\Delta V)$ for all zipping lengths

$$\frac{C_L'(\Delta V)}{C_1'(\Delta V)} < 0.1 \tag{27}$$

Neglecting the contribution of $C_L'(\Delta V)$, and noting that the change in liquid volume $\Delta V_L = -\Delta V$, we obtain:

$$\frac{dC(\Delta V)}{d\Delta V} \approx -\frac{dC_1(\Delta V_L)}{d\Delta V_L} = \frac{6\,\varepsilon_F}{h\,t_F} \frac{R}{c+2R} \approx \frac{6\,\varepsilon_F}{h\,t_F} \frac{c+l}{3c+2l} \tag{28}$$

The last expression assumes moderate volume changes, so that R is close to its initial value $c+l$, which results in a constant $C_1'(\Delta V)$. This holds within few percent for our numbers. For large actuator sizes and small slope of the top electrode the contribution of C_L' increases and should be included in eq. (28). Within the same "moderate changes" approximation $R = c + l$ the derivative is modified as follows:

$$C' = C_1' + C_L' \approx \frac{6\,\varepsilon_F\,(c+l)}{h\,t_F\,(3c+2l)} \left(1 - \frac{(c+2l)}{(c+l)} \frac{t_F\,\varepsilon_L}{h\,\varepsilon_F} \ln \left(\frac{h\,\varepsilon_F}{t_F\,\varepsilon_L} \right) \right) \tag{29}$$

---

[7]SI units are used here, and for brevity ε_0 is included into all permittivities. The unzipped capacitance is calculated assuming two-layer capacitor with slowly varying liquid thickness t_L.

Displaced volume and the critical voltage

Substituting the result (28)[8] into the equality (6) together with the eq. (14) gives an analytic approximation for the equilibrium condition.

$$\frac{3 \times 2^5}{\pi^3} \frac{\mu\, t_{\mathrm{M}}}{a} \left(\frac{V_0 + \Delta V}{a^3}\right)^3 = \frac{6\,\varepsilon_{\mathrm{F}}}{h\, t_{\mathrm{F}}} \frac{c + l}{3c + 2l} \frac{U^2}{2} \tag{30}$$

From here we obtain the dependence of the displaced volume on the applied voltage:

$$\Delta V = a^3 \left(\frac{U}{U_{\mathrm{c}}}\right)^{2/3} - V_0 \tag{31}$$

Here, we defined the characteristic voltage U_{c}, which combines the majority of the system properties, but is separated from the basic scaling with respect to the aperture size a and the initial volume V_0.

$$U_{\mathrm{c}} = \left(\frac{2^5}{\pi^3} \frac{h\, t_{\mathrm{M}}\, t_{\mathrm{F}}}{a\, \varepsilon_{\mathrm{F}}} \frac{3c + 2l}{c + l} \mu\right)^{1/2} \tag{32}$$

Equation (31) produces negative displaced volume ΔV for small voltages, which is forbidden by system's design. This means, that zipping does not start below some threshold (critical) voltage U_0:

$$U_0 = U_{\mathrm{c}} \left(\frac{V_0}{a^3}\right)^{3/2} \tag{33}$$

For small voltages $U < U_0$, the equilibrium state remains completely unzipped due to the initial filling V_0.[9]

Dependence of the focal length on voltage

Now we can relate the lens volume $V = \Delta V + V_0$ to its focal length f, and obtain its dependence on voltage. We use the thin lens expression $f = \rho/(n-1)$ for a plane-convex spherical cap of radius $\rho = (a^2 + Z^2)/2Z$, assuming small volume (lowest order in $Z/a << 1$). Here, n is the refractive index of the lens (paraffin oil). This is a good approximation for our system, which results in a simple relation:[10]

$$f(V) \approx \frac{\pi a^4}{4(n-1)} \frac{1}{V} \tag{34}$$

Together with the eq. (31), the focus-voltage relation for voltages $U > U_0$ becomes:

$$f(U) = \frac{\pi a}{4(n-1)} \left(\frac{U_{\mathrm{c}}}{U}\right)^{2/3} \tag{35}$$

For voltages below the threshold value, the focal distance remains unchanged and equal to its initial value $f(U < U_0) = f(V_0) = f_0$.

---

[8]The more accurate expression (29) with the corresponding changes was used in actual calculations, which modifies the result by a few percent.

[9]The situation is similar to Peano-HASEL actuators under a constant load [6]. For $U < U_0$ the free energy expression (5) has a minimum at $V_0 \neq 0$, $\Delta V = 0$, which has *positive derivative* with respect to ΔV.

[10]In a more detailed approach, one can develop parametric formulas, based on the full volume and pressure expressions (8), (10) and *thick* lens formulas for the focal length.

Relations between a deflected laser beam and the focal length

When a thin laser beam, parallel to the optical axis, enters the lens at the radial distance d_x from the axis, it is deflected by the angle β. This can be approximately treated as a single light ray. It hits the screen (positioned at a distance d_s behind the lens) at the distance y from the optical axis. These quantities are related to the focal length of the lens by:

$$\tan \beta = \frac{d_x}{f} \tag{36}$$

$$y = d_x \left(\frac{d_s}{f} - 1 \right) \tag{37}$$

When the focal length of the tunable lens changes by $f_2 - f_1 = \Delta f$, the tangent and the spot position on the screen change accordingly:

$$\Delta \tan \beta = \tan \beta_2 - \tan \beta_1 = -d_x \frac{\Delta f}{f_1 \, f_2} \tag{38}$$

$$\Delta y = y_2 - y_1 = d_s \, \Delta \tan \beta = -d_x \, d_s \frac{\Delta f}{f_1 \, f_2} \tag{39}$$

Therefore, the *relative* changes in $\tan \beta$ and spot position with respect to the reference state (1) are proportional to the relative change in focal length with respect to state (2).

$$\frac{\Delta \tan \beta}{\tan \beta_1} = -\frac{\Delta f}{f_2} \tag{40}$$

$$\frac{\Delta y}{y_1} = -\frac{\Delta f}{f_2} \frac{d_s}{d_s - f_1} \tag{41}$$

Both expressions do not depend on d_x, which simplifies the experimental measurements.

Cost estimation and scalability

A single small lens costs about $0.1431 \, €$ (calculation is given in Supplementary Table 3). The price is mostly determined by the PDMS elastomer, which makes $96\,\%$ of the total costs. The use of the elastomer could be readily reduced or replaced depending on the specific application or available fabrication facilities. Of course, the costs can be greatly reduced by the economies of scale as well. The lenses are scalable without changing the fabrication methods, as the lens body is molded and the polymer foils (laser) cut to dimensions. We note however that miniaturizing the lenses to the mm scale would require a change to fabrication schemes that are assisted by high precision machines.

Optimizing homogeneous zipping

The models derived above assume axial symmetric zipping of the polymers. However, variabilities of opening angles or initial distance of the polymer lead to inhomogeneous zipping in the experimental realization. We here use two approaches to better control the start and propagation of the zipping fronts.

Welding points: Regular separated welding points at the circumference of the actuator induce starting points for zipping, due to a locally reduced separation of the electrodes (Supplementary Fig. S4). As a rule of thumb, the distance between the welding points along the circumference should be (appreciably) smaller than twice the width of the zipping annulus. Likewise, in the presence of auxiliary concentric rings (see below), it should be smaller than twice the distance between these

rings. Increasing the number of welding points could lead to more homogeneous zipping, however only if the welding points are homogeneous as well. An infinite amount of points –hence a continuous circular welding– in practice still results in inhomogeneous zipping as certain regions of the welding will be (slightly) thinner and hence a (uncontrolled) starting point of a zipping front. Single points give better control over where the zipping starts.

Concentric rings: Concentrically patterned electrodes influence the zipping front propagation by inducing an anisotropy in radial direction. While the welding points represent a start of a zipping front, the concentric rings adjust the propagation speed of the zipping front. As we observed that the start of zipping fronts is much more important for homogeneous zipping than the propagation speed (at least for our lens dimensions), we disregarded the option of having concentric rings alone early in the design phase of the lenses.

Future work will investigate the influence of those approaches to optimize zipping of ZEAP actuators. Non circular electrodes, such as regular polygons, might also greatly enhance the zipping behaviour. Recent work suggests that edges act as starting points for zipping as well [7].

Towards ZEAP actuators with operating voltages <50 V

The characteristic voltage in eq. (32) relates to the operating voltages of ZEAP devices. Omitting weak influence of the actuators lateral size parameters c and l eq. (32) can be simplified to

$$U_{\mathrm{c}} \sim \left(\frac{\mu\, t_{\mathrm{M}}\, h\, t_{\mathrm{F}}}{a\, \varepsilon_{\mathrm{F}}} \right)^{1/2} \tag{42}$$

The remaining quantities can be divided into actuator parameters (h, t_{F}, ε_{F}) and lens membrane parameters (a, t_{M}, μ), but all parameters influence the characteristic voltage in similar extent. A reduction of t_{F} by a factor of 4 halves the operating voltages, as does a 4-times increase of ε_{F}. For the current design parameters $U_{\mathrm{c}} = 4.6\,\mathrm{kV}$, $3.1\,\mathrm{kV}$ for the small and large actuators respectively, which results in operating voltages $<500\,\mathrm{V}$. Keeping the macroscopic lateral geometry unchanged, the cumulative design parameters would need to be changed by a factor 100 to achieve a reduction of operating voltages to $<50\,\mathrm{V}$. This is possible by using softer membranes ($\mu^{*} = \mu/\sqrt{10}$) and foils with reduced thickness ($t_{\mathrm{F}}^{*} = t_{\mathrm{F}}/\sqrt{10}$) and higher permittivity ($\varepsilon_{\mathrm{F}}^{*} = 10\varepsilon_{\mathrm{F}}$).

Supplementary Tables

Author/ company	Lens material type	Actuation	Aperture (mm)	Minimum focal length (mm)	Maximum focal length (mm)	Driving voltages (V)
This work	liquid/ elastomer	electroactive zipping (EAZ)	6	22	550	<500
D. Wang *et al* [8]	liquid	electrowetting	15	15	165	<53
J. Wang *et al* [9]	liquid	electrowetting	6	19.2	265	<75
Jin *et al* [10]	liquid	inhomogeneous electric field	3	4.9	19.3	<52
Xu *et al* [11]	liquid	inhomogeneous electric field	3.5	-8.28	-4.4	<120
L. Wang *et al* [12]	elastomer	reshaping ring	1	950	∞	<5000
Bae *et al* [13]	elastomer	reshaping ring	1.5	3.8	22.3	–
Choi *et al* [14]	elastomer	reshaping ring	1.5	3	24.5	<400
Optotune 10-42-OF [15]	liquid	reshaping ring	10	-500	500	3.3
Wapler *et al* [16]	liquid/ solid	piezo electric	7.6	-142	167	–
Cheng *et al* [17]	liquid/ elastomer	electro hydraulic	6	24.5	690.3	<8000
Wirthl *et al* [18]	liquid/ elastomer	dielectric elastomer	20	32	67	<6500
Maffli *et al* [19]	liquid/ elastomer	dielectric elastomer	5	30.8	37.9	<3000
Carpi *et al* [20]	liquid/ elastomer	dielectric elastomer	7.6	16.72	22.73	<3500
Nam *et al* [21]	elastomer	dielectric elastomer	3	14.3	23.7	<4600

Table S1 | Overview of tunable lens systems and their performances.

| Parameter	Notation	Unit	Small actuator	Large actuator
Pressure	p	kPa	0.2 - 200	
Aperture radius	a	mm	3	
Lens membrane thickness	t_{M}	mm	0.2	
Membrane prestretch	λ_0	–	1.0	
Inner actuator radius	c	mm	5	
Actuator length	l	mm	3	10
Outer radius	$c+l$	mm	8	15
Actuator height	h	mm	0.4	0.2
Zipping foil thickness	t_{F}	µm	6	
Zipped electrode length	l_1	mm	0 - 2.5	0 - 9.5
Young's modulus PDMS	$E = 3\mu$	MPa	2.9	
Poisson's ratio PDMS	ν	–	0.5	
Refractive index paraffin oil	n	–	1.48	
Rel. permittivity paraffin oil	ε_{L}	–	3	
Rel. permittivity PET	ε_{F}	–	2.2	

Table S2 | Simulation parameters for the experimentally realized lenses. The values $n \neq \sqrt{\varepsilon_{\mathrm{L}}}$, as the permittivity is given for the quasi static case, while the refractive index refers to the optical frequencies.

Material	Quantity	Price (€/kg)	Costs (ct)
PDMS	0.8 g	171 €/kg	13.71 ct
Paraffin oil	62 µL	45.2 €/kg	0.28 ct
Copper	0.54 mg	5800 €/kg	0.32 ct
6 µm-thick PET foil	4 cm²	–	< 0.01 ct
Total	–	–	14.3 ct

Table S3 | Material costs estimation. A single small lens costs about $0.1431\,€$. The price is mostly determined by the PDMS elastomer, which contributes to $96\,\%$ to the total costs. Prices are taken for typical research scale quantities ($\sim 1\,$kg or $1\,$L packages).

Supplementary Figures
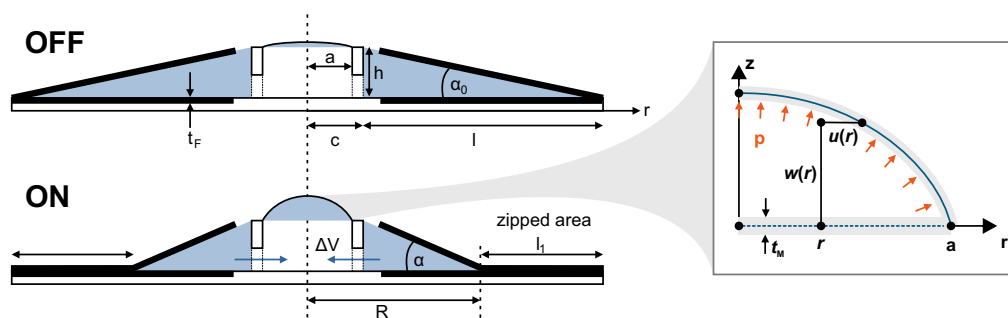
Figure S1 | Geometry parameters of a tunable lens. The volume ΔV displaced from the actuator into the lens, inflates the membrane. A point at position r is displaced by $w(r)$ in z-direction and $u(r)$ in lateral direction.
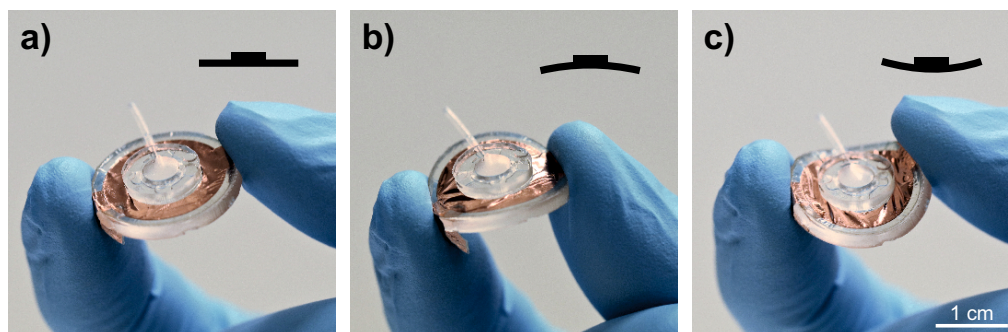

Figure S2 | Bending of soft tunable lenses. a) Flat tunable lens based on ZEAP actuators. The overall lens body is made of majorly soft materials and thin polymer foils. **b, c)** The lenses are bendable and compressible, which allows safe handling of the devices.
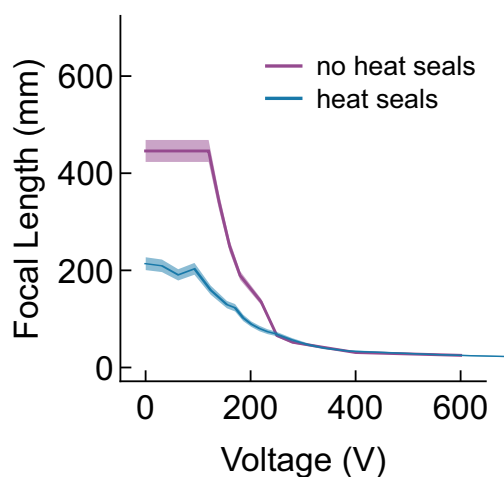

Figure S3 | Effect of heat seals. Comparison of lenses with large actuators featuring heat seals and no heat seals. Focal length changes require higher voltage in the initial regime (<300 V) when no heat seals are used. The focal length at higher voltages are unchanged. Note that the plateau, marking the threshold voltage, is at different initial focal length due to different initial fillings. The shape of the curves differs due to the effect of the heat seals (compare with Fig. 2g).
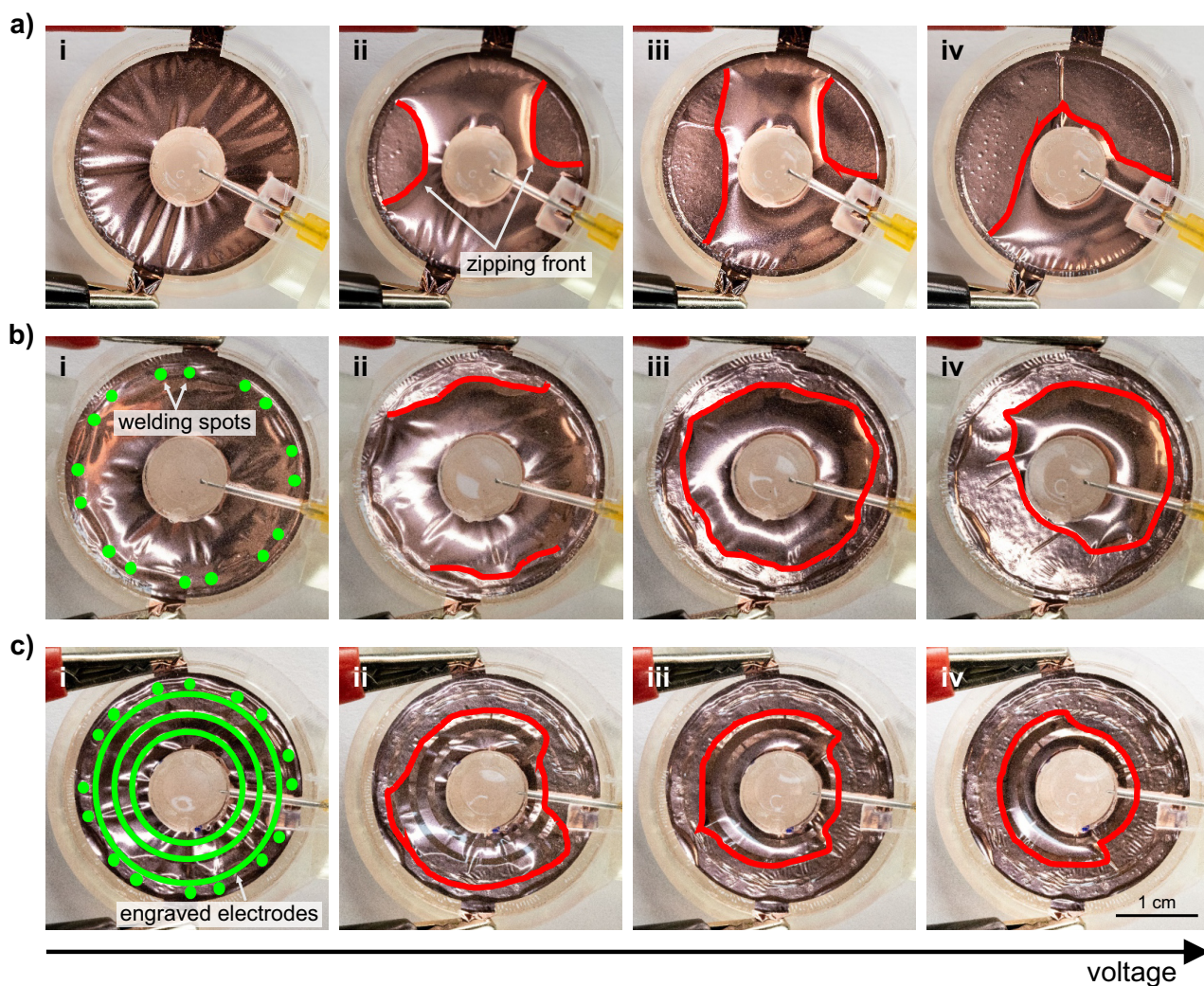
Figure S4 | Controlling the zipping behaviour. a), For large unstructured electrodes, zipping is not concentric and leads to partial inflation of the electrodes. The applied voltage increases from (i) to (iv). **b)**, Welding points facilitate the concentric zipping around the lens (iii). Still, zipping is dominant at specific sites (iv). **c)**, Additional concentric rings, engraved into the top electrode lead to more axially symmetric zipping. The rings are electrically connected via small copper traces left between them.
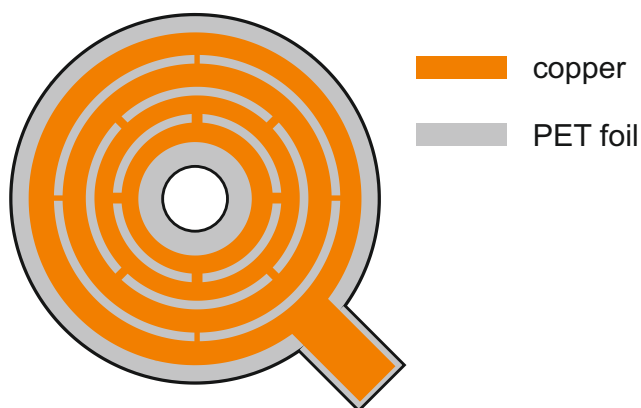

Figure S5 | Concentric rings pattern. A pattern of rings is laser-engraved into the copper electrodes to enhance concentric zipping.
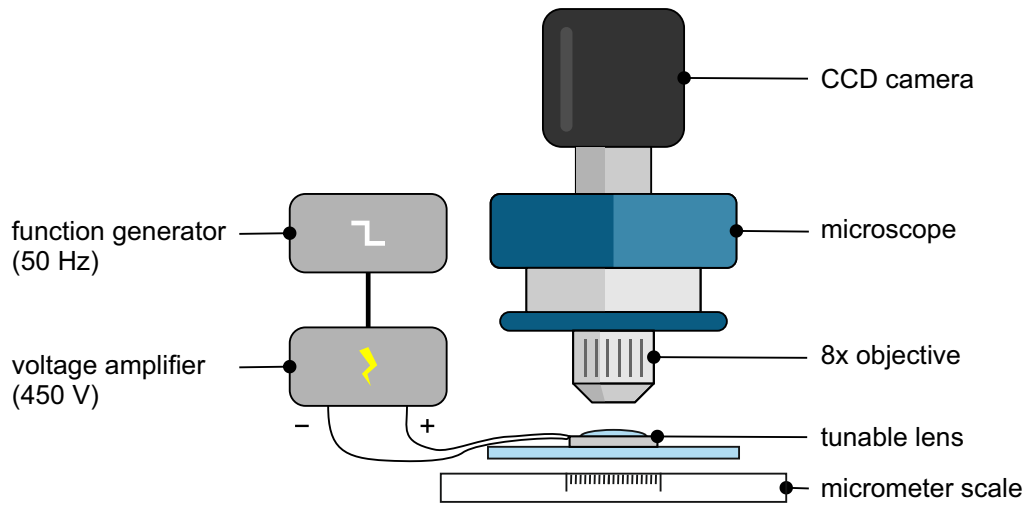
Figure S6 | Setup for focal length measurement. The tunable lens is positioned under a microscope with fixed distance to a micrometer-scale serving as image. The focal length of the tunable lens is calculated from the measured magnification. Abbreviations: CCD, charge coupled device.
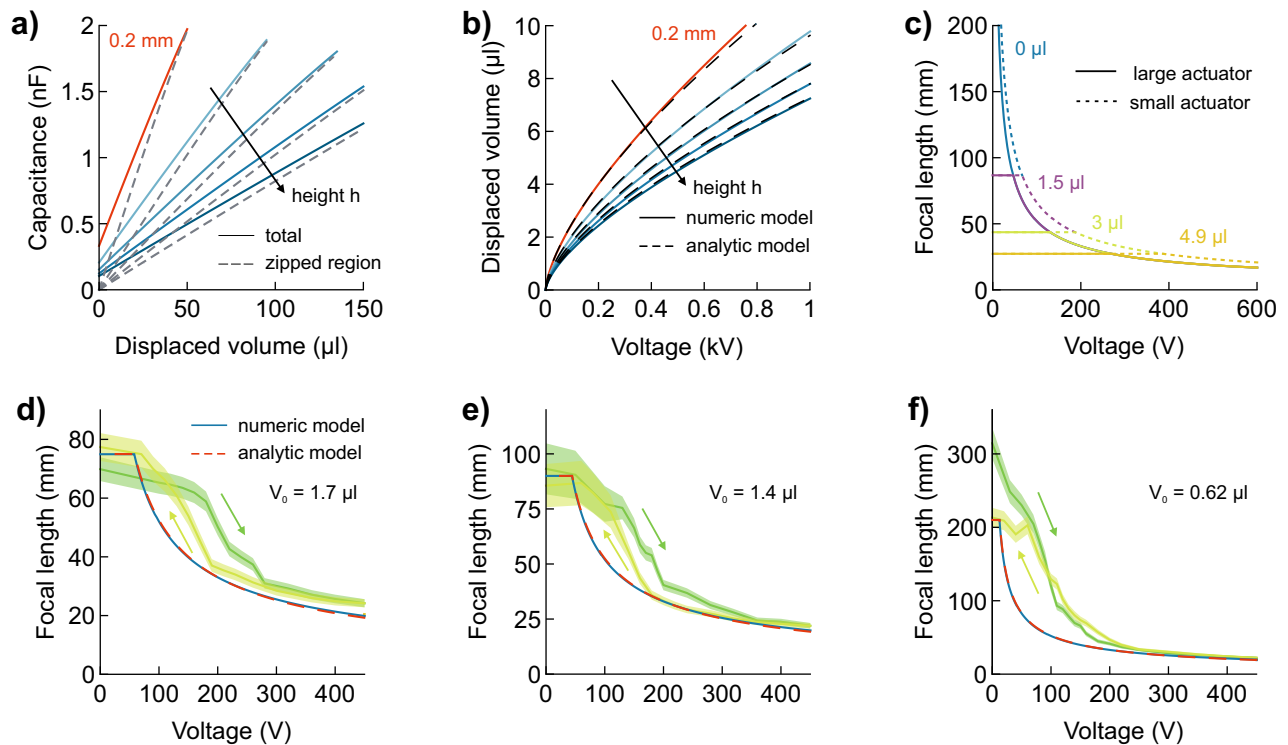
Figure S7 | Lenses with large actuators. a), The total capacitance of zipped and unzipped electrodes relates nearly linearly to displaced volume. Dashed lines represent the contribution of the zipped region. Characteristics are calculated for different actuator heights (0.2 (chosen height, red), 0.4, 0.6, 0.8, 1 mm). **b)**, The balance of mechanical and electrostatic forces results in the displaced-volume-voltage relations, with good agreement between the numerical (solid) and analytic (dashed) models **c)**, Combination of actuator and lens properties results in focus-voltage characteristics. The initial filling volume determines starting (maximal) focal length and the threshold voltage for focal length tuning. Lenses with a small actuator (dashed lines) require slightly higher operating voltages due to a larger initial opening angle compared to lenses with a large actuator (solid lines). **d)** - **f)**, Measured focal-length-voltage characteristics in comparison with the analytic (red dashed) and numerical (blue solid) models for lenses with different initial fillings. The experimental curves below and near the threshold voltages are influenced by effects that stem from non-uniform foil thickness due to welding spots or non-concentric zipping.

13
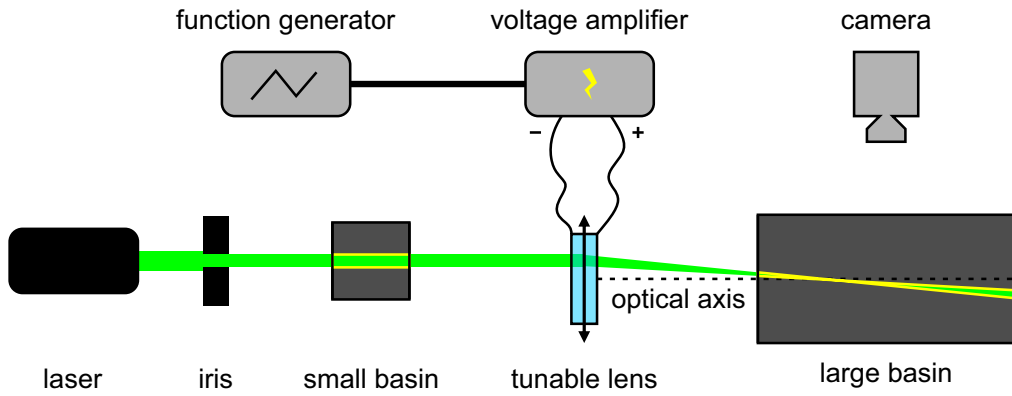
Figure S8 | Setup for dynamic response measurements. A laser beam is projected through a lens and two rhodamin-filled basins parallel to the optical axis at a fixed offset. The changing deflection of the laser beam is tracked with a camera at 50 frames per second.
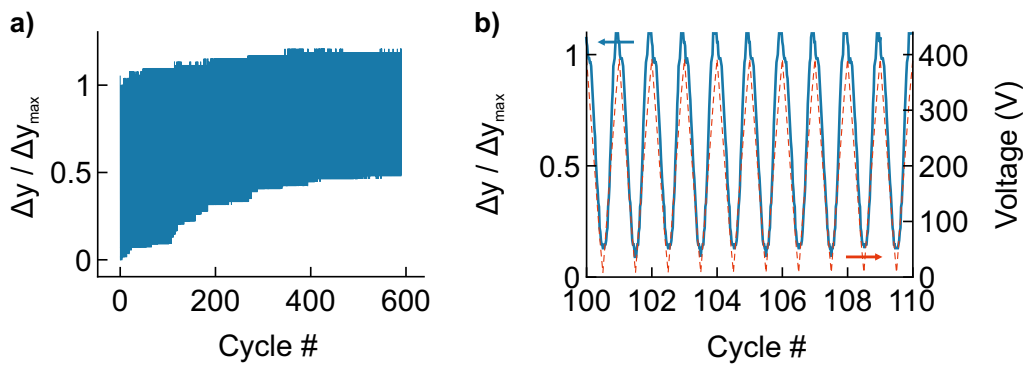
Figure S9 | Cyclic performance. a) Cyclic actuation of ZEAP tunable lenses shows small drifts and a slightly reduced performance after 600 continuous actuation cycles. **b)** The lens response follows the driving voltage, which is triangular in shape and changes polarity at every second cycle. No delamination of the PET foils can be observed over the course of the experiments.

References

[1] R. Baumgartner, A. Kogler, J. M. Stadlbauer, C. C. Foo, R. Kaltseis, M. Baumgartner, G. Mao, C. Keplinger, S. J. A. Koh, N. Arnold, et al. *Advanced Science* **2020**, *7*, 5 1903391.

[2] P. Rothemund, S. Kirkman, C. Keplinger. *Proceedings of the National Academy of Sciences* **2020**, *117*, 28 16207.

[3] Z. Suo. *Acta Mechanica Solida Sinica* **2010**, *23*, 6 549.

[4] C. Keplinger, M. Kaltenbrunner, N. Arnold, S. Bauer. *Proceedings of the National Academy of Sciences* **2010**, *107*, 10 4505.

[5] P. Pokornỳ, F. Šmejkal, P. Kulmon, P. Novák, J. Novák, A. Mikš, M. Horák, M. Jirásek. *Applied optics* **2017**, *56*, 34 9368.

[6] N. Kellaris, V. G. Venkata, P. Rothemund, C. Keplinger. *Extreme Mechanics Letters* **2019**, *29* 100449.

[7] E. Leroy, R. Hinchet, H. Shea. *Advanced Materials* **2020**, *32*, 36 2002564.

[8] D. Wang, C. Liu, Q.-H. Wang. *Optics express* **2019**, *27*, 7 10058.

[9] J.-H. Wang, X. Zhou, L. Luo, R.-Y. Yuan, Q.-H. Wang. *Optics Communications* **2019**, *445* 56.

[10] B. Jin, H. Ren, W.-K. Choi. *Optics Express* **2017**, *25*, 26 32411.

[11] M. Xu, D. Xu, H. Ren, I.-S. Yoo, Q.-H. Wang. *Journal of Optics* **2014**, *16*, 10 105601.

[12] L. Wang, T. Hayakawa, M. Ishikawa. *Optics Express* **2017**, *25*, 25 31708.

[13] J. W. Bae, E.-J. Shin, J. Jeong, D.-S. Choi, J. E. Lee, B. U. Nam, L. Lin, S.-Y. Kim. *Scientific reports* **2017**, *7*, 1 1.

[14] D.-S. Choi, J. Jeong, E.-J. Shin, S.-Y. Kim. *Optics express* **2017**, *25*, 17 20133.

[15] Optotune, **accessed: 13.07.2020**. URL https://www.optotune.com/el-10-42-of-lens.

[16] M. C. Wapler. *Optics Express* **2020**, *28*, 4 4973.

[17] X. Cheng, M. Yu, J. Ma, B. Li, Y. Zhang, P. Wang, Z. Jiao. *Smart Materials and Structures* **2020**, *29*, 4 045017.

[18] D. Wirthl, R. Pichler, M. Drack, G. Kettlguber, R. Moser, R. Gerstmayr, F. Hartmann, E. Bradt, R. Kaltseis, C. M. Siket, et al. *Science advances* **2017**, *3*, 6 e1700053.

[19] L. Maffli, S. Rosset, M. Ghilardi, F. Carpi, H. Shea. *Advanced functional materials* **2015**, *25*, 11 1656.

[20] F. Carpi, G. Frediani, S. Turco, D. De Rossi. *Advanced functional materials* **2011**, *21*, 21 4152.

[21] S. Nam, S. Yun, J. W. Yoon, S. Park, S. K. Park, S. Mun, B. Park, K.-U. Kyung. *Soft robotics* **2018**, *5*, 6 777.